SSCL-N-851

SSCL-N-851
June 1994
Distribution Category: 400

G. Snitchler
R. Jayakumar

Summary of HEB Magnet Ramp Rate Studies

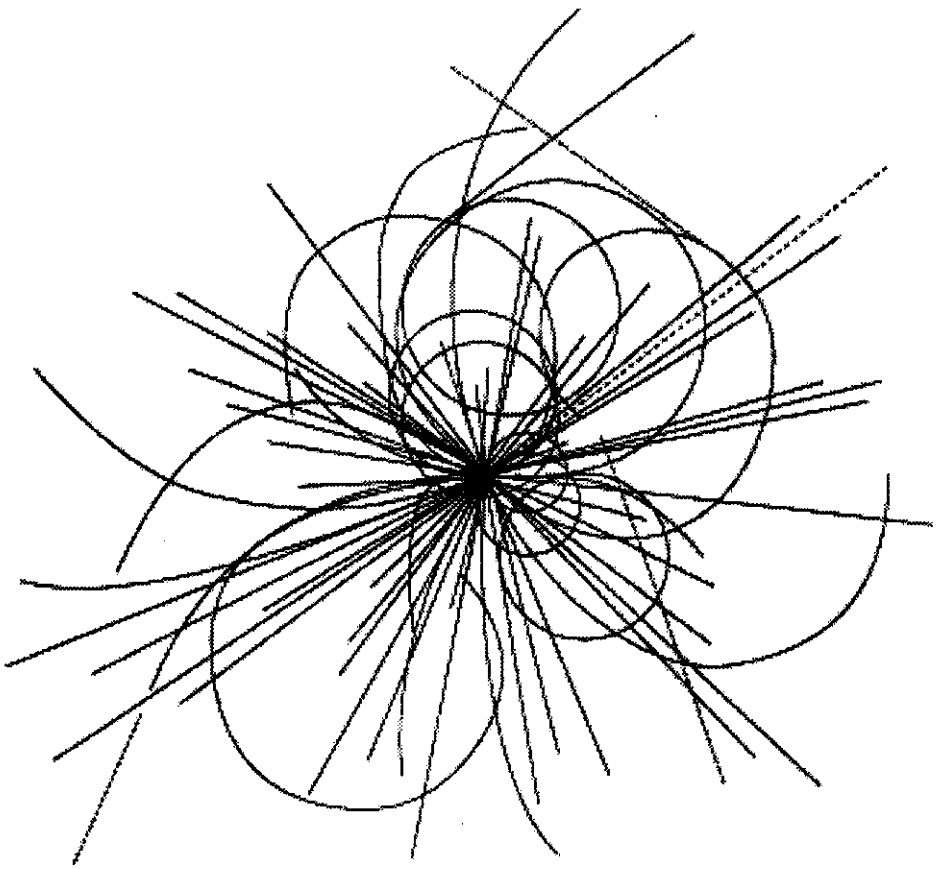

Superconducting Super Collider Laboratory

Disclaimer Notice

This report was prepared as an account of work sponsored by an agency of the United States Government. Neither the United States Government or any agency thereof, nor any of their employees, makes any warranty, express or implied, or assumes any legal liability or responsibility for the accuracy, completeness, or usefulness of any information, apparatus, product, or process disclosed, or represents that its use would not infringe privately owned rights. Reference herein to any specific commercial product, process, or service by trade name, trademark, manufacturer, or otherwise, does not necessarily constitute or imply its endorsement, recommendation, or favoring by the United States Government or any agency thereof. The views and opinions of authors expressed herein do not necessarily state or reflect those of the United States Government or any agency thereof.

Superconducting Super Collider Laboratory is an equal opportunity employer.

SSCL-N-851

Summary of HEB Magnet Ramp Rate Studies

G. Snitchler and R. Jayakumar

Superconducting Super Collider Laboratory*
2550 Beckleymeade Ave.
Dallas, TX 75237 USA

June 1994

*Operated by the Universities Research Association, Inc., for the U.S. Department of Energy under Contract No. DE-AC35-89ER40486.

Summary of HEB Magnet Ramp Rate Studies

G. Snitchler and R. Jayakumar

Superconducting Super Collider Laboratory
2550 Beckelymeade Ave.
Dallas, TX 75237

Abstract

A significant amount of ac loss and ramp rate quench sensitivity data was generated in the ASST CDM program, the General Dynamics model magnet program, and the Westinghouse model magnet program. Several models were generated to explain the ramp rate behavior. A summary of relevant data and models is presented.

1.0 INTRODUCTION

The High Energy Booster (HEB) is a bipolar machine ramping at 62 A/s. It requires eight bipolar cycles to fill the collider ring. A single bipolar cycle is shown in Figure 1 and includes 203 s of ramp time and 29 s of stop time per half cycle.

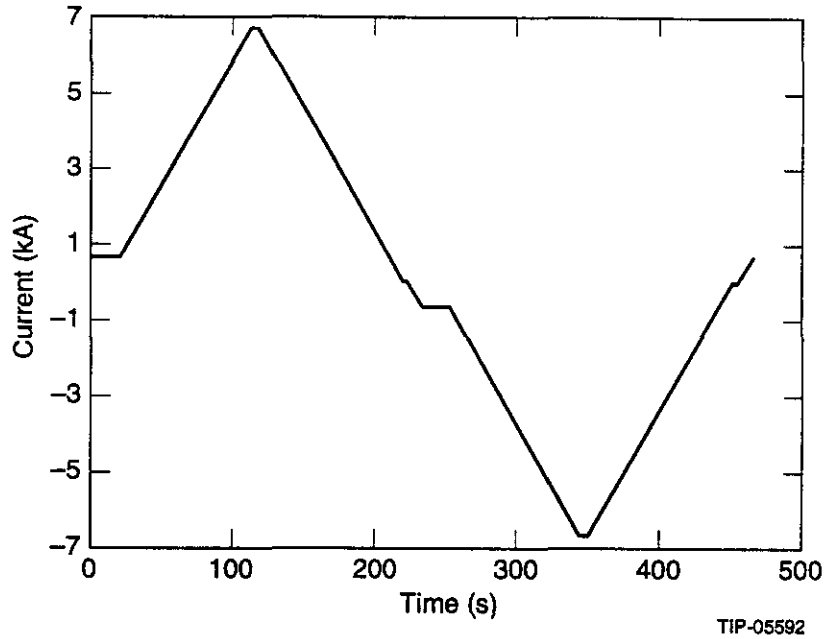

Figure 1. Baseline HEB bipolar ramp cycle.

The HEB ramp cycle is considered to be dynamic when compared to collider ring operation in which the dipole magnets endure only a 4 A/s ramp to operational current. The HEB magnets may require a more robust design specifically for ac operation. The ac loss mechanisms include hysteresis and eddy current terms. The superconductor hysteresis magnetization can be approximated by bulk superconductor magnetization

$$M_s = \frac{2\mu_o}{3\pi} J_c d_f \left(1 - \frac{J}{J_c}\right) \tag{1}$$

and iron magnetization M_h is the standard M vs. H loop. The energy dissipated is

$$Q = \frac{1}{\mu_o} \int_0^{B_m} M dB. \tag{2}$$

The eddy current losses for strand and conductor are related to the eddy current time constant and the eddy current magnetization is

$$M_e = 2\tau \frac{dB}{dt} \tag{3}$$

where the strand the time constant is[1]

$$\tau = \frac{\mu_o}{2\rho_{et}} \left(\frac{L}{2\pi}\right)^2 . \tag{4}$$

The power generated is

$$W_e = \int \frac{2\tau}{\mu_o} \left(\frac{dB}{dt}\right)^2 dV . \tag{5}$$

The well known expression for Rutherford cable the power per unit length generated is and scaling laws can be derived from Morgan's formula.[2]

$$W_e l = \frac{N^2 h^2 L}{60R} \frac{dB}{dt} . \tag{6}$$

A baseline trade study was conducted using information from the 40-mm CDM prototype program, magnetization data, and sample data from Brookhaven and KEK.[3,4] See Table 1. The baseline average heat load for the HEB cycle was 11.5 Watts including pause states.[5]

Table 1. Baseline ac loss estimate per meter of dipole magnet.

SC HYSTERESIS (J)	IRON HYSTERESIS (J)	STAND EDDY (J/A/S)	CABLE EDDY (J/A/S)
128	25	0.18	0.08

2.0 RAMP RATE SENSITIVITY

The primary ramp pattern utilized in most SSCL magnet single magnet test procedures was a sawtooth ramp from zero to quench current at several ramp rates from 1 A/s to 300A/s. This ramp cycle was selected because it was easy to implement and was justified by thermal arguments. The longest thermal time constant in the *x-y* plane of a dipole magnet was approximately 100 s. In addition, there is a thermal time constant associated with the annular flow of helium which is in the range of 200-400 s. The only additional thermal information gained by establishing a pre-conditioning ramp cycles would be the annular flow pre-heating. The quench current as a function of ramp rate has been studied in several dipole magnet programs. In Figures 2, 3, and 4, the FNAL prototype magnets made with IGC, Oxford, and Supercon cable quench performance is presented, respectively.[6] There is a clear distinction between the IGC magnet performance when compared to the magnets constructed by other manufacturers. The Brookhaven ramp rate studies for the glass-epoxy and all polyamide magnet are shown in the Figures 5 and 6, respectively.[7]

The short magnet ramp rate behavior is distinctive from the long magnet programs. The ramp rate quench sensitivity for the FNAL 40-mm aperture magnet program is plotted in Figure 7. These magnets are interpreted as low loss type A magnets in a pool boiling environment. See the discussion in section 4.1.[8] The FNAL-and SSCL-built 50-mm short magnets are shown in Figures 8 and 9. In general, these magnets reveal vaguely type B behavior assumed to be associated with trapped currents.

The General Dynamics and Westinghouse model magnet programs provided additional and unique ac information. The General Dynamics model magnets, labeled DSD, were fabricated with the all polyamide material XMPI[9] and cured above a temperature of 225°C. The original development of XMPI for accelerator magnets was carried out at Brookhaven with great care for the temperature and pressure profiles. This implementation and the selection of cable from a vendor which typically yields type B magnets yielded medium loss and ramp sensitive magnets shown in Figure 6.

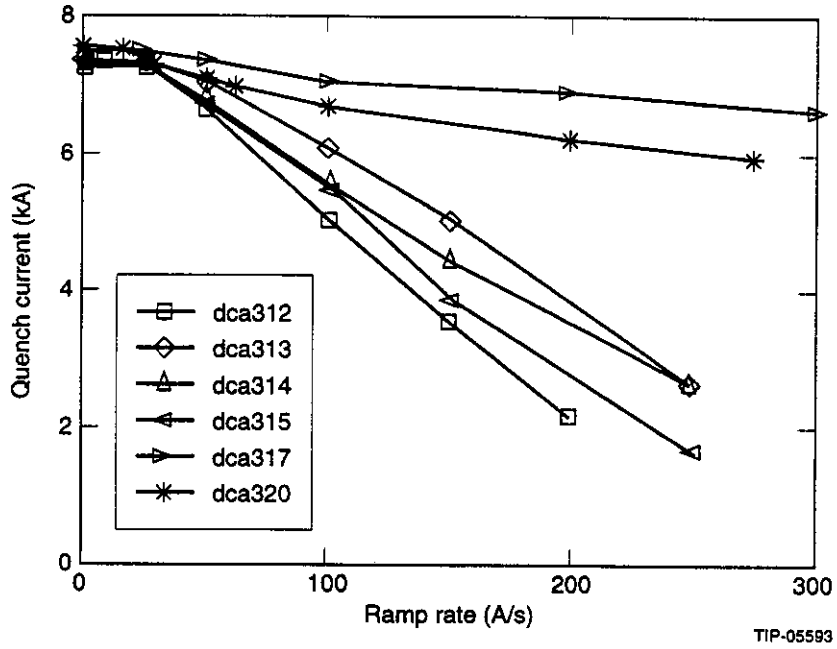

Figure 2. FNAL magnets constructed with IGC cable.

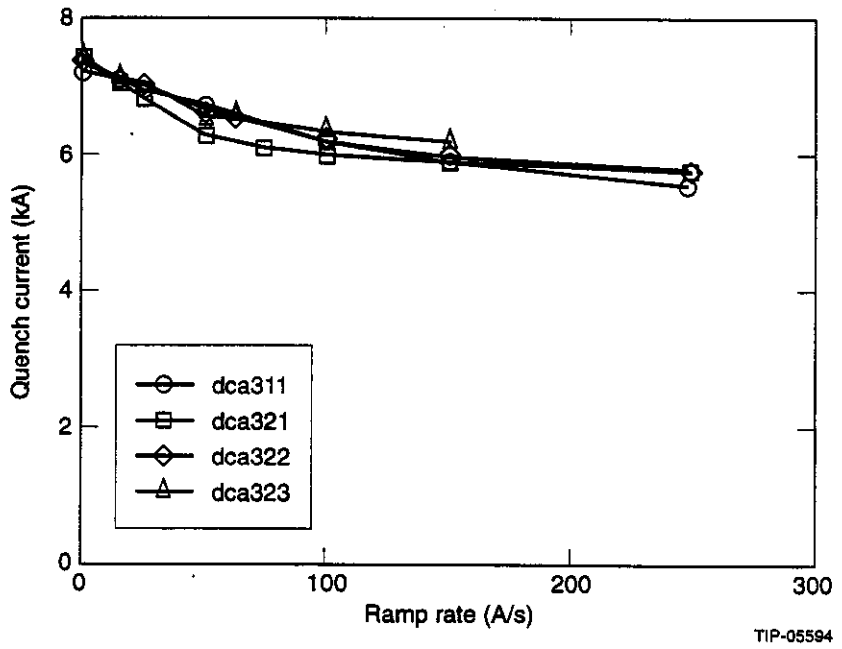

Figure 3. Ramp rate performance of the FNAL magnets made with Supercon cable.

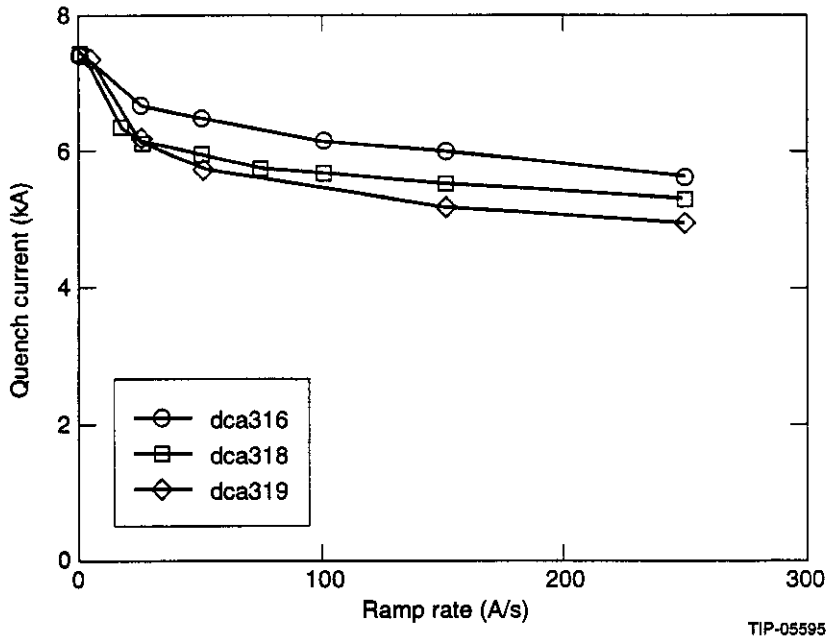

Figure 4. Ramp rate performance of the FNAL magnets made with Oxford cable.

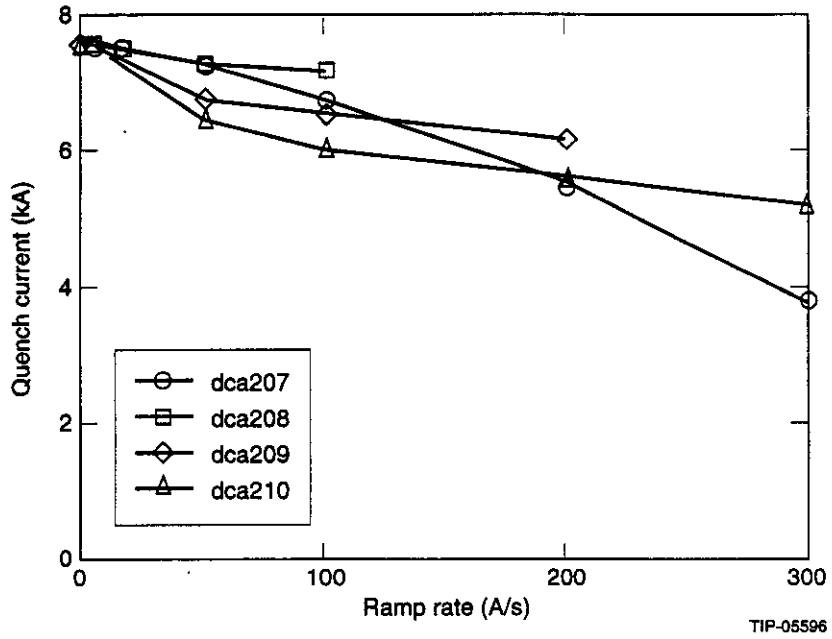

Figure 5. Ramp rate performance of the BNL glass-epoxy magnets.

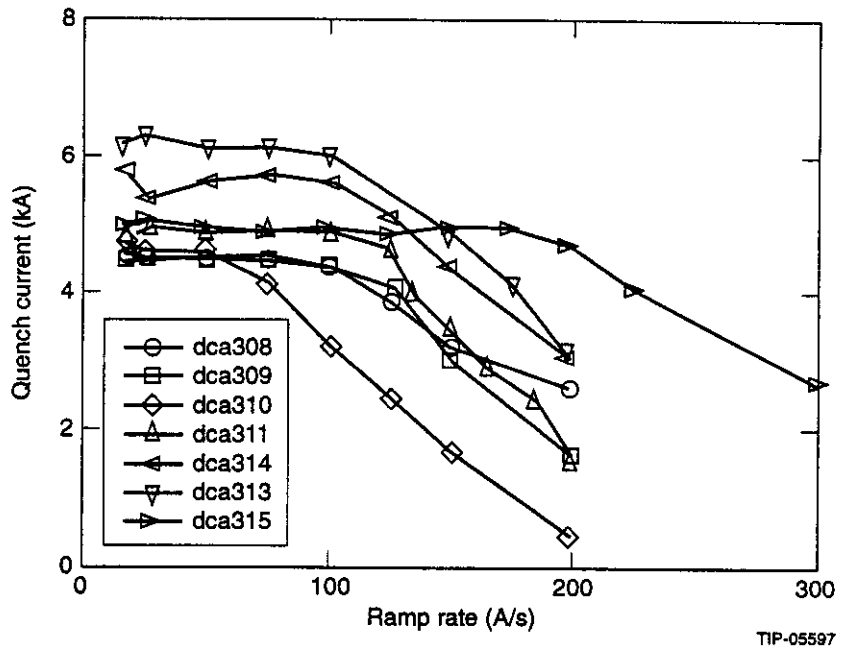

Figure 6. Ramp sensitivity of the 40-mm FNAL series model magnets.

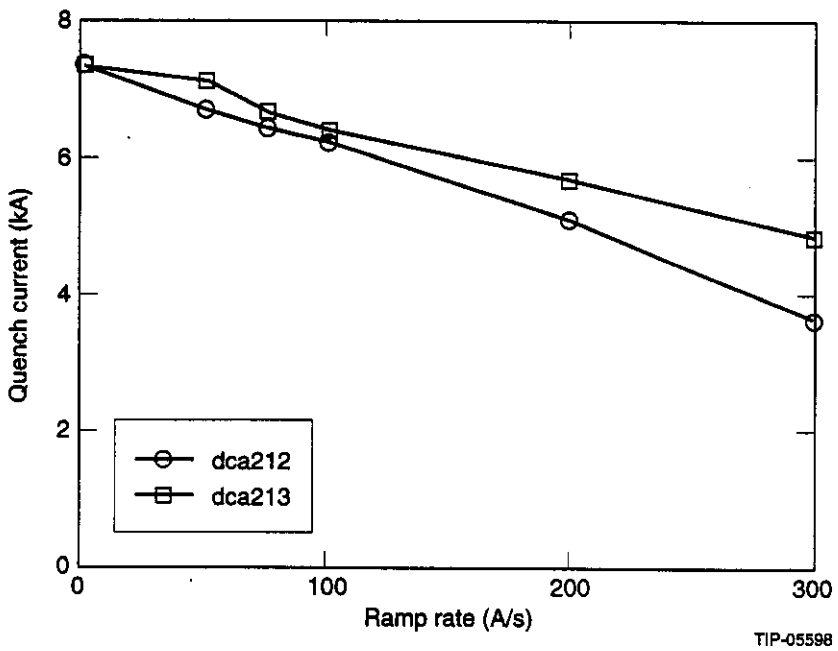

Figure 7. Ramp rate performance of the BNL all polyamide magnets.

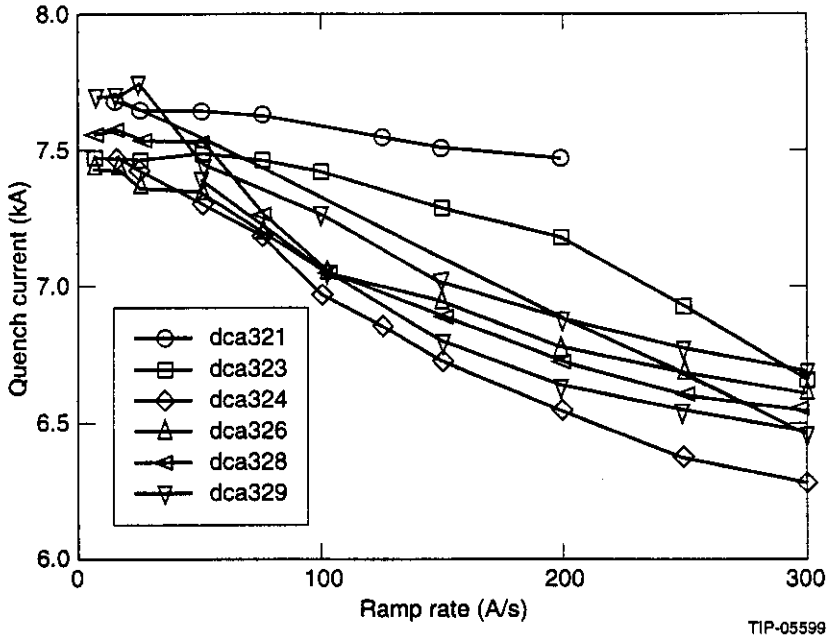

Figure 8. Ramp sensitivity of the 50-mm FNAL series model magnets.

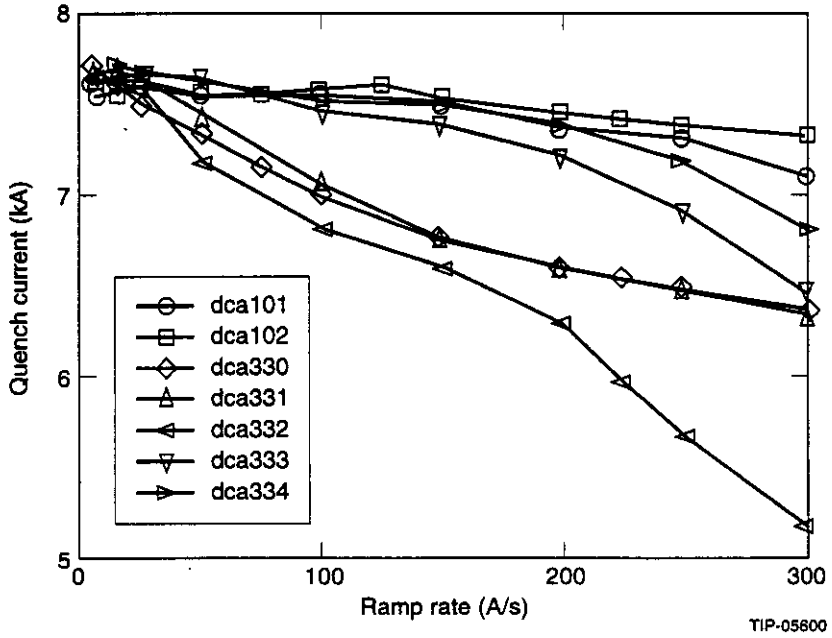

Figure 9. Ramp sensitivity of the post ASST 50-mm FNAL and SSCL model.

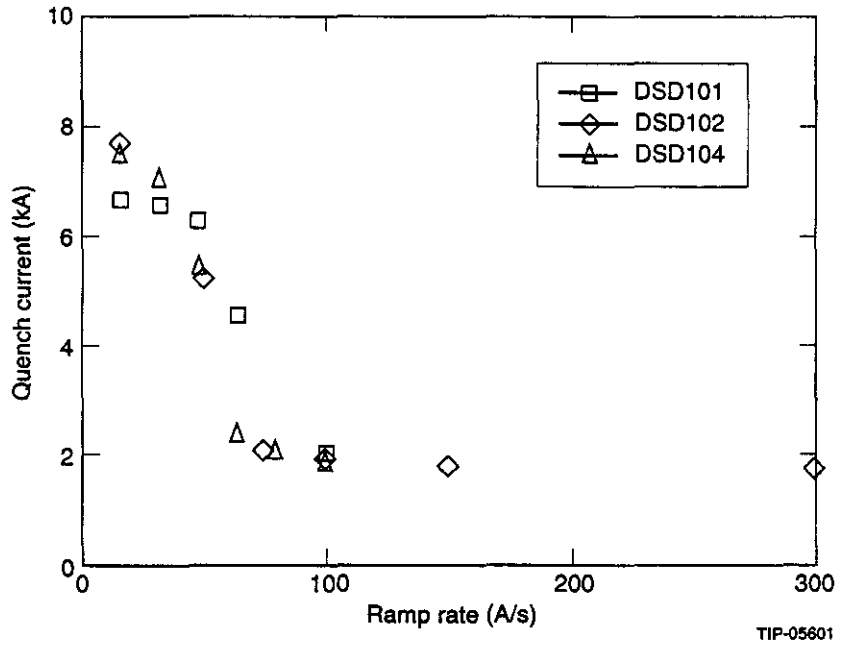

Figure 10. Ramp sensitivity of the DSD series model magnets.

The General Dynamics magnets were fabricated with FNAL-style curing to a fixed size using Brookhaven insulation and curing temperatures believed to be near 250°C. The curing pressures were higher than nominal because the cross-section was magnetically designed using ASST glass-epoxy dimensions which are smaller than the XMPI two 50% overlap cable dimensions. As a consequence of some or all of the above parameters, the DSD magnets were the most ramp sensitive magnets observed in any of the Super Collider development programs as shown in Figure 10.[10–12]

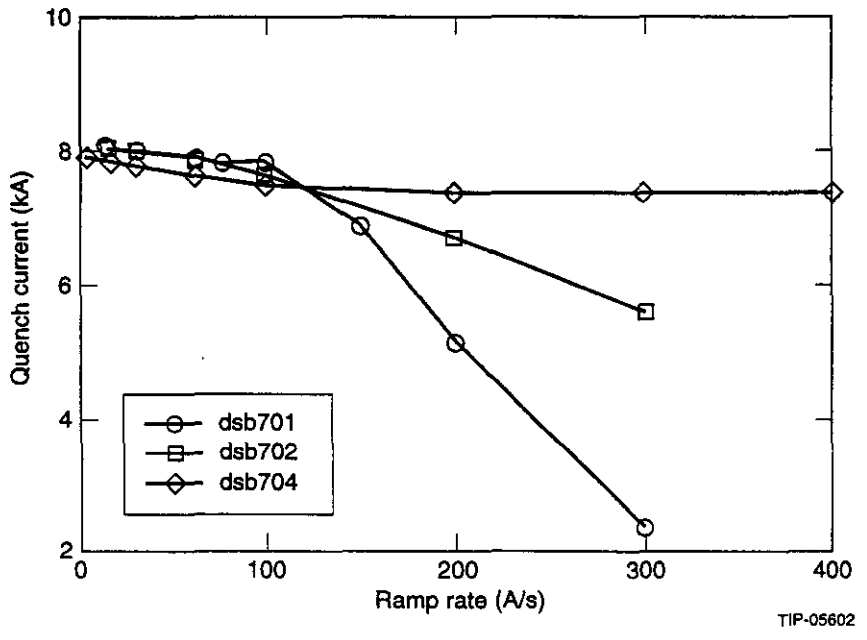

Figure 11. Ramp sensitivity of the DSB series model magnets.

The Westinghouse model magnet program was unique for two reasons: One, the magnet was constructed using a coil-on-coil wind and cure technique similar to HERA magnets[13] and two, there was a conscious effort to implement all-ebonal cable in DSB703. The coil-on-coil curing procedure requires two cure cycles on the inner coil. This may increase the risk of ac sensitivity by increasing the heat treatment time. DSB701 appears to be a high loss magnet based on ramp rate data shown in Figure 11 and no EIEO ac loss measurements were available because the measurements were outside to high-voltage protection circuits.[14] DSB702 had significantly lower ramp rate sensitivity than DSB701 and this may be associated with more control over curing pressures.[15] DSB703 is a unique type B magnet which is assumed to be directly associated with the high interstrand resistance enforced by the ebonal coating on the strands.[16]

3.0 AC LOSS MEASUREMENTS

The ac loss integral technique or energy-in-energy-out (EIEO) was developed at FNAL.[17,18] In summary, the energy loss is defined as

$$U = -\oint V(t)I(t)dt = -\oint \left[\int_0^t V(t)dt - LI(t) - LI(0) \right] dI \tag{7}$$

where the terms in the bracket are the "corrected voltages" plotted in Figures 2–4. Reference 4 has more information on the technique used to analyze the voltage and current data. The data is acquired by HP3458A meters with a data rate of 5.8 Hz. Generally, five monopolar loops are performed to provide a limited statistical basis for the area in VI loop. The waveform is shown in Figure 12.

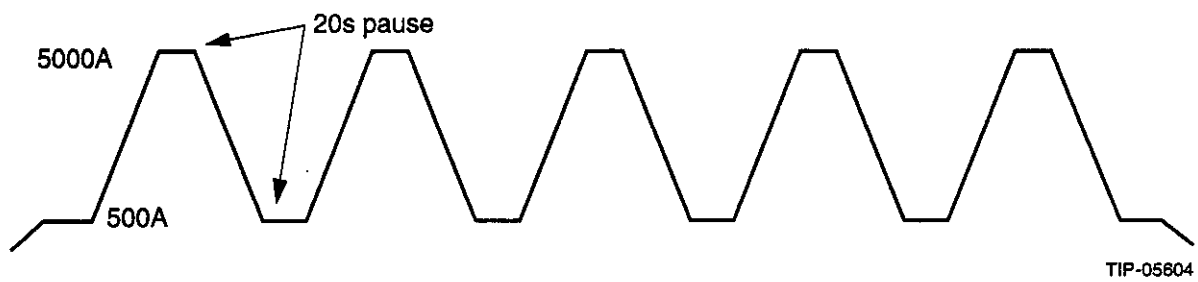

Figure 12. Ramp waveform.

Long time constants were observed in the VI loops for DSD102, DSD103, and DSD104 magnets. A sample of the long time constant behavior is plotted in Figure 13.[19] In the 50 A/s case notice that the turn around voltage at 0.5 and 5 kA has an exponential character which appears to be an eddy current inductance loop discharging and charging in the opposite direction. Long time constants were also observed in magnetic measurements of the DSD model magnets.[20]

In Figure 14, there is a plot of loss vs. ramp rate. It is clearly non-linear as a function of ramp rate. We interpret this effect as the lowering of the area in the VI loop at faster ramp rates due to the eddy current charge up time. In an attempt to quantify the non-linear behavior, a second fit was made to the first three data points which is labeled fit (b).

A summary of all magnets measured at FNAL and SSCL is listed in Table 2. The authors took the liberty to classify the magnets as type A, high loss magnets, or type B, low loss and trapped current magnets. In some cases the criteria for A vs. B is poorly defined. Only the DSD magnets are known to have the significantly non-linear ac loss behavior.

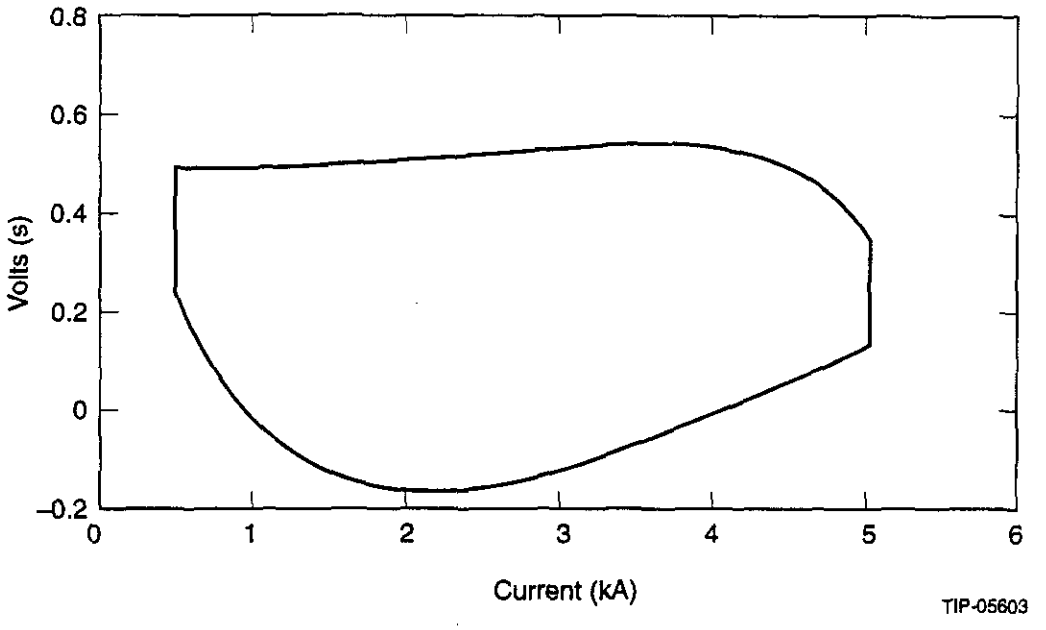

Figure 13. DSD103 VI loop at 50A/s.

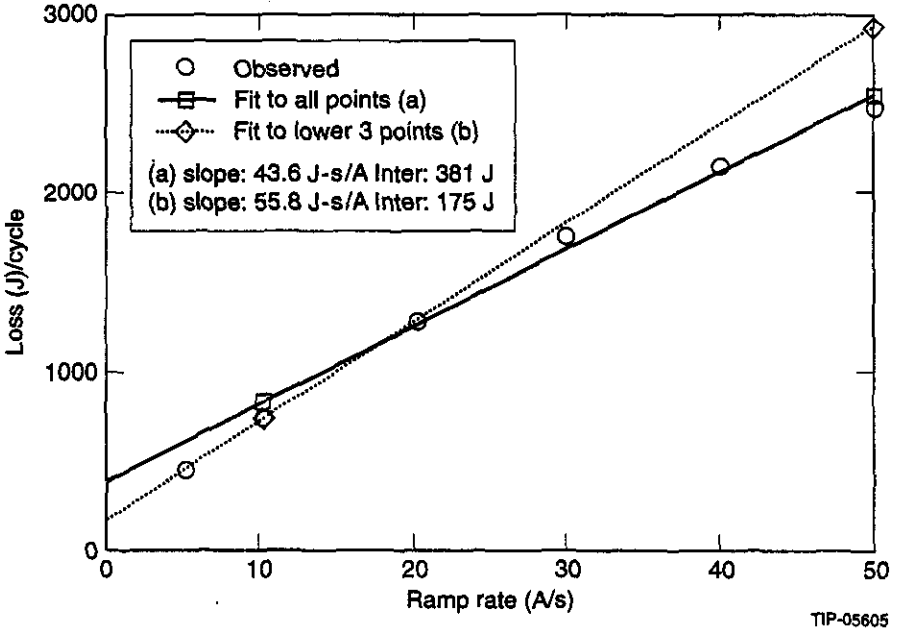

Figure 14. Summary of DSD103 ac loss behavior.

Table 2. Ac loss measurements per unit meter of magnet.

MAGNET	CABLE VENDOR	HYSTERESIS LOSS (J)	EDDY LOSS (J/A/S)	TYPE
FNAL 15m				
DCA311	Supercon	49.6	0.80	B
DCA312	IGC	49.27	4.20	A
DCA314	IGC	50.60	2.38	A
DCA315	IGC	51.27	3.31	A
DCA318	Oxford	48.2	0.50	B
DCA319	Oxford	47.53	0.62	B
FNAL 1.5 m				
DCA323		64.00	0.41	B
DCA324		61.33	0.41	B
DCA328		66.67	0.42	B
DCA329		64.67	0.42	B
GD 1.8 M				
DSD102	IGC	180	22.86	A
DSD103	IGC	117	37.2	A
DSD104	IGC	129	39.8	A
WEC 1.8 m				
DSB702	IGC	187	1.15	A
DSB703	IGC(ebonal)	192	0.58	B

4.0. MODELS

4.1 Thermal Models

A finite element thermal model was developed using ANSYS to compute the quench currents based on a ΔT associated with a transient heat load. In some of the model cases, an approximation for global heating has been implemented by introducing a changing bath temperature, *Tb*, from results of a finite element thermal model,[21–22] and is expressed as

$$T_b = 0.306p\left[1-\mathrm{Exp}\left[-\frac{t}{117.5}\right]\right]+0.0744P\left[1-\mathrm{Exp}\left[\frac{t}{3.1}\right]\right]+4.65(10^{-4})Pt+0.060 \tag{8}$$

where the exponential terms represent the coil to bypass and coil to annular flow time to steady state time constants. The linear term is the global heating of the He due to eddy currents. The constant term is the global heating due to hysteresis. The power/meter of magnet straight section generation is defined as

$$P=\left(1.36(10^{-3})+6.32(10^{-4})f\right)\left(\frac{dT}{dt}\right)^2 \tag{9}$$

where f is the scaling factor for measured interstrand eddy current losses relative to an initial estimate of 0.08 (Js/Am) in Table 1 of Reference 5 which is the value for half of a bipolar cycle to 6.5 kA. Table 2 in Reference 3 is a reduction of the observed losses in a monopolar ramp from 500 to 5000 and returning to 500 A. The scaling factor can be derived from

$$f=\frac{E\left(\frac{6.5}{4.5}\right)-0.18}{0.08} \tag{10}$$

where E is the eddy current loss in Table 2 of Reference 5. For example, the largest loss magnet, DCA312, has a scaling factor of 74 and a typical type B magnet has a scaling factor of 8.9. There is harmonic evidence DCA312–DCA315 could have significant asymmetry in azimuthal heat loading which may impact the azimuthal temperature profile. An ANSYS model was performed with head loading information provided by Ogitsu[23] and no significant change in resultant profile was evident.[24]

4.2 Strand Stability Model

A model for the critical current of a superconducting strand under changing current and magnetic field conditions was developed by R. Mints.

In this work,[25–26] the electric field parallel (Epar) and perpendicular (Eperp) to the strand (assumed to be a uniform matrix of superconducting filamanets and normal conducting material) are calculated for conditions of (a) transport current $I_t = 0$, $dB/dt \neq 0$, (b) $dI_t/dt \neq 0$, $dB/dt = 0$ and (c) $I_t \neq 0$, $dB/dt \neq 0$. The real magnet case of $dI_t/dt \neq 0$ and $dB/dt \neq 0$ is obtained by linearly summing cases (b) and (c). The relations for the case (a) are obtained in a similar way as in Reference 3. For the case (a), the (saturated) region of supercurrents (Epar $\neq 0$) are banana shaped regions at the edges of the strand with thickness which depends on dB/dt and the critical current density and a characteristic time constant that depends upon the normal matrix transverse resistivity. The azimuthal component of the supercurrent due to the fact that the filaments are twisted then circulate (closed) through the matrix (Epar = 0, Eper $\neq 0$) . For this case Epar is negligible or small compared to Eperp. It is pointed out that the rate for the operating ramp rate of the magnet, the assumption of uniform matrix is poor. For the case (b) and (c), the penetration of the supercurrents is cylindrically symmetric so that these currents flow in a shell, so that Maxwell's equations can be solved more directly to get the electric fields. In the case (b) parallel electric field is much larger than the perpendicular component. The case (c) is obtained by combining (a) and (b), so that the spatial distribution of the supercurrent (saturated) region is a shifted shell, so that value of Epar depends upon the azimuthal position around the strand. For the limiting case (d) of $dI_t/dt \neq 0$ and $dB/dt \neq 0$ which respresents strands in the coils of a magnet, the results of (b) and (c) are linearly added to obtain Epar.

Electric fields obtained as above for case (d) are used to calculate the critical current of a strand under ramping conditions. The field value is compared with the stability condition,

$$Epar \leq (Ph/Ax_S)(j_1/j_C)\{1/(dj_C/dt)\} \tag{11}$$

where A and P are area and cooled perimeter of the strand, x_S is the volume fraction of superconductor, h is the heat transfer coefficient, j_1 is a parameter describing superconducting critical surface and j_C is the critical current density.

$$(1.5\, i_m + (1-i_m)^{3/2} - 1) / (1-0.5\, i_m) - \beta\, [i_m + \ln(1-i_m)] = \alpha \tag{12}$$

where $\alpha = (dI_q/dt) / (dI/dt)$, $\beta = 3\mu_0/(8NkR)$, $dI_q/dt = (3\pi/x_S)(h/NkR^2)(j1/jc)\{1/(djc/dt)$

N is the number of turns and $B = Nk\,I$. The critical current is calculated for different values of α and β and for $\beta << 1$ a serious degradation of critical current occurs for $\alpha << 1$. For SSC conductors a serious degradation of critical current would occur for 25 A/s if h is less than 0.1 W/m^{2}K. The model shows that critical current drops initially with increasing ramp rate and then decreases more slowly as ramp rate is increased.This is similar to the B type magnet behavior although the model predicts much larger slopes or a severe degradation for heat transfer coefficient expected in SSC magnets.

4.3 Eddy Current Stability Model

This eddy current loop model[28] consists of one eddy current loop of two adjacent parallel strands which charge and decay according to the equation:

$$\frac{dI_e}{dt} = \frac{\left(\frac{d\Phi}{dt} - rI_e\right)}{L}. \tag{13}$$

The loop resistance, r, is the sum of the contact resistance, r_c, and the current sharing resistance, $r_S = p(rrr,B,T)\chi(rrr,B,T,I_t)\frac{1}{A}$ where χ is the current sharing function which varies linearly as a function of T between 0 and 1 in the current sharing region and has the value of zero below current sharing and the

value of one above the critical current for a given total current, I_t, magnetic induction, B, and temperature, T. χ is computed by using the Morgan Jc surface and a binary search subroutine to find the beginning of current sharing and critical currents. The routine then determines

$$\chi(rrr,B,T,I_t)=\left[\frac{T}{T_c-T_{cs}}-\frac{\begin{matrix}0;(T\le T_{cs})\\ T_{cs}\\ T_c-T_{cs}\\ 1;(T\le T_c)\end{matrix}}{}\;;(T_{cs}\le T\le T_c)\right]. \tag{14}$$

The electrical circuit is then coupled to a simple representation of the thermal domain seen by the strand carrying the transport plus eddy current. The strand temperature is governed by

$$\frac{Al_q}{\gamma c_p}\frac{dT}{dt}=Al_q\rho J^2\chi(rrr,B,T,I_t)-hPl_q(T-T_b) \tag{15}$$

where the Joule heating term has the current sharing function. The local temperature domain, T, is considered to be the strand plus local helium which is current sharing over a length, l_q. The external domain is considered to be adjacent strands and the temperature is labeled, Tb.

The pulsing eddy current model was abandoned because the time constant required to have a stable pulse was too small when compared to the special ramp studies performed on the ASST magnets. These studies were labeled Schermer ramps, Snitchler V-ramps, and Ogitsu-Krzywinski ramps.[6–7]

4.4 Trapped Current Models

The trapped current models were developed to explain the long time constant behavior which clearly could not be associated thermal time constants. The trapped current models fall into two classes: 1) Turck models and 2) diamond models. The Turck models are well described in Reference 27 and will not be discussed in this paper.

The second class of models address opposed pairs of strands which carry trapped currents. The trapped current could be caused by a net emf occurring at the end turn region or by disturbances associated with local low interstrand resistances. There are uncompleted models from Wake, Snitchler, Swenson, Akhmetov, Kovachev, Carr, and probably others at the time of this publication.

As an example, a simple LR circuit model can be constructed. The trapped and transport current can be computed at any time by

$$I_t=\frac{v}{r_t}\left(1-\mathrm{Exp}(-t\frac{r_t}{L_t})\right)+Rt \tag{16}$$

where v is the emf, r_t is the resistance between the two strands, L_t is the total inductance of the two strand circuit, and R is the transport strand ramp rate. The parameters selected for the calculation in Figure 15 is $L_t = 600 \times 20 \times 10^{-9}$ and $r_t = 80 \times 10^{-9}$. The inductance for one loop is computed to be 20×10^{-9} so there are 600 loops active in this model.

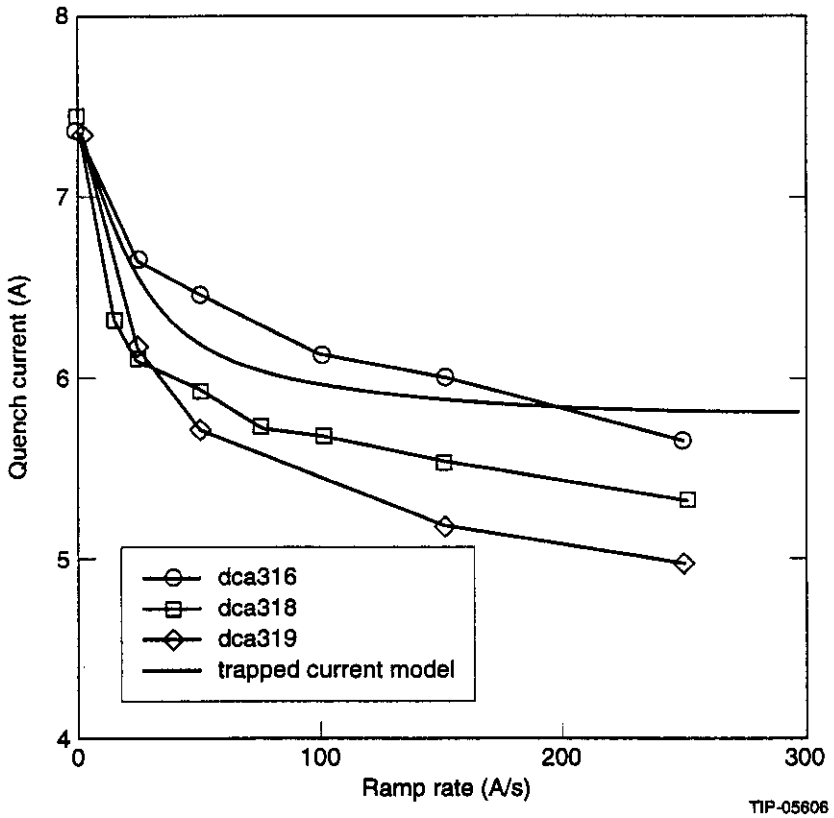

Figure 15. Trapped Current Model.

4.5 Field Harmonic Models and Quench Localization

The dynamic magnetic field harmonics provided a useful tool for understanding high loss behavior. In particular, DCA312 was successfully mapped out for local areas of high eddy current. These axial positions in the magnet were then mapped out for azimuthal contributions to identify the source of the high eddy current contributions.[29] The quenches were then localized by a quench antenna.[30]

The data from these two programs were then used to develop an autopsy program where the interstrand resistances were measured in extracted sections of collared coil.[31] The measurements by Kovachev demonstrated that adjacent strands had a much lower interstrand resistance than normal strand crossings. There is work in progress to study the adjacent strand resistances and develop a model to describe this effect.[32]

5.0 UNRESOLVED ISSUES

At the termination of the Supercollider project there are still many unanswered questions. The trapped current models appear to be the most promising explanation but no final conclusions or program to verify the models are available. The type A behavior can be mitigated by a higher interstrand resistance but, higher interstrand resistances can drive type B behavior. A well planned study of controllable resistances should be implemented with further studies of strand coatings: ebonal, chromium, solder, or other more innovative resistance barriers.

REFERENCES

1. Wilson, "Superconducting Magnets," Oxford Press (1983).
2. G. Morgan, "Eddy Current losses in Rutherford Cable," *J. Appl. Phys.*, (1973).
3. A. Ghosh, "Workshop on Persistent Current Magnetization," Brookhaven National Laboratory (1989).
4. V. Kovachev, "Trip Report for Foreign Travel to KEK, Japan," internal SSCL document (1992).
5. G. Snitchler, V. Kovachev, D. Orrell, and J. Jayakumar, "Design Considerations for a 60 mm HEB dipole magnet," SSCL-374 (1992).
6. J. Tompkins, electronically distributed quench summary reports from the SSCL long magnet test team at Fermilab.
7. J. Muratore, electronically distributed quench summary reports from Brookhaven National Laboratory.
8. M. Wake, private communication.
9. R. Bailey, "Preliminary Design Review for the Collider Dipole Magnet," presented at General Dynamics Space Systems Division, San Diego, CA (1992).
10. C. Haddock, R. Bird, G. Snitchler, R. Garlow, and P. Reddy, "DSD102 Model Dipole Test Results," MSD Technical Document MD-MJG-0-93-008.
11. C. Haddock, R. Bird, G. Snitchler, R. Garlow, and P. Reddy, "DSD103 Model Dipole Test Results," MSD Technical Document MD-MJG-0-93-010.
12. C. Haddock, R. Bird, G. Snitchler, R. Garlow, and P. Reddy, "DSD104 Model Dipole Test Results," MSD Technical Document in preparation.
13. G. Snitchler, *ed.*, "DSB design book," Internal SSCL Magnet Division document MD-MJG-O-94-030.
14. C. Haddock *et al.* "DSB701 Model Dipole Test Results," MSD Technical Document MD-MJG-O-93
15. C. Haddock *et al.* "DSB702 Model Dipole Test Results," MSD Technical Document MD-MJG-O-93
16. C. Haddock *et al.* "DSB703 Model Dipole Test Results," MSD Technical Document MD-MJG-O-93
17. S. Delchamps, R. Hanft, T. Jaffery, W. Kinney, W. Koska, M.J. Lamm, P.O. Mazur, D. Orris, J.P. Ozelis, J. Strait, and M. Wake, "AC Loss Measurement of SSC Dipole Magnets," Proceedings of the Applied Superconductivity Conference at Fermi National Acclerator Laboratory (1992).
18. S. Delchamps, R. Hanft, T. Jaffery, W. Kinney, W. Koska, M.J. Lamm, P.O. Mazur, D. Orris, J.P. Ozelis, J. Strait, and M. Wake, "AC Loss Measurement of SSC Dipole Magnets," *Proceedings of Workshop on AC Superconductivity*, KEK proceedings 92-14, National Laboratory for High Energy Physics, Tsukuba, Japan (1992).
19. G. Snitchler, C. Haddock, and M. Wake, "Analysis of the DSD Model Magnets for AC Loss Behavior," MSD Technical Document MD-MJG-O-93-013.
20. Y. Zhao, T. Ogitsu, A. Devred, "DSD Magnetic Measurements," MSD Technical Document MD-TA-25.
21. B. Aksel *et al.* "Evaluation of Cooling Performance for Possible HEB Dipoles," MSD Internal Document MD-ENG-92-A-004 (1992).

22. G. Snitchler, *et al.*, "Heat Generation and Cooling of SSC Magnets at High Ramp Rates," Proceedings of the IFCA Workshop on AC Superconductivity, Tsukuba, KEK Proc. 92-14, (1992), p. 15-18.

23. T. Ogitsu, private communication (the more recent work is listed in Reference 29).

24. R. Schermer and G. Snitchler, "Predicting Temperature Rise During Magnet Ramping," MSD Internal Document MT-TA-247.

25. R. Mints, "Electrical Field Distribution in a Superconducting Multifilamentry Strand," MSD Internal Document MD-TA-248.

26. R. Mints, "Current Carrying Capacity of a Superconducting Multifilamentry Strand," MSD Internal Document MD-TA-249.

27. Turck, *J. Appl. Phys.* **50** (8), p. 5397 (1979).

28. G. Snitchler, R. Schermer, presentation on the pulsing eddy current model at an Westinghouse MSIM (1992).

29. T. Ogitsu, "Influence of Cable Eddy Currents on the Magnetic Field of Superconducting Particle Accelerator magnets," SSCL-N-848 (1994).

30. A. Devred *et al.*, "About the Ramp Sensitivity of SSC Dipole Magnets," MSD Internal Document MD-TA-268 (1994).

31. V. Kovachev, "Interstrand Resistance of DSA328 Cal," SSC-637 (1993). Also see, SSCL-651 (1993).

32. V. Kovachev and W. Carr, work in progress.